EXPRESSION OF SLC4A11, CLAUDIN 4 AND OTHER CELL MEMBRANE TRANSPORTERS IN THE MAMMALIAN RENAL MEDULLA AND THEIR PHYSIOLOGICAL IMPLICATIONS

By

MICHAEL THOMAS GEE

_____

A Thesis Submitted to The Honors College

In Partial Fulfillment of the Bachelors degree
With Honors in

Physiology

THE UNIVERSITY OF ARIZONA

M A Y 2 0 1 9

Approved by:

_____

Dr. Thomas Pannabecker
Department of Physiology

Abstract

The kidneys play a vital role in maintaining solute homeostasis in mammals. One way the kidneys can regulate solute concentrations is through the urine concentrating mechanism. Although advancements have been made to elucidate the general functions of different kidney regions, the medulla is not as well understood. The goal of this study is to examine the architecture and expression of specific proteins in the mammalian medulla. A tight junction protein called claudin-4 has been shown to be expressed in rat medullary collecting ducts, thin ascending limbs (TALs) of Henle's Loops, and potentially in aquaporin-1 (AQP1) negative descending thin limbs (DTLs) of Henle's Loops. Meanwhile, the transporter protein SLC4A11 has been found to be expressed in primarily the DTLs and potentially in other structures in both mice and rat kidneys. Additionally, three-dimensional reconstruction of the tubules in the pig medullary region has been performed. These findings not only provide us with several potential biomarkers that can be used to study the mammalian renal medulla, but also provide some insight into the different transport processes that occur in the renal medulla.

Introduction

One of the important roles of the mammalian kidney is the production of urine to maintain salt concentrations and fluid volume. To accomplish this, the kidney is comprised of many nephrons which serve as the functional units of the kidney. Each nephron possesses functionally distinct segments that span specific regions of the kidney. These nephrons can be categorized into two types, long-loop nephrons and short-loop nephrons based on how deep the nephron forms its bend (Figure 1). Both nephron types possess different properties and, in addition to the presence of other distinct nephron segments, help to delineate the different regions of the kidney.

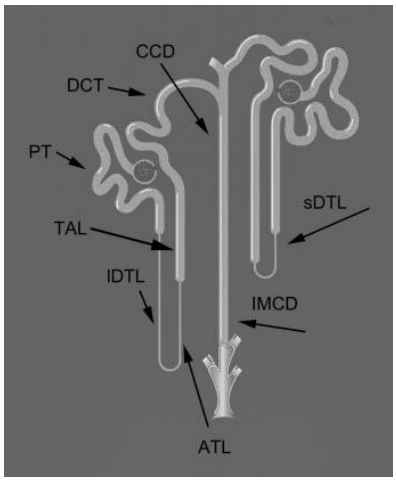

Figure 1. Basic structure of the nephron with specific segments labeled. On the left is a long-loop nephron with the proximal tubule (PT), long-loop descending thin limb (lDTL), thick ascending limb (TAL), and distal convolute tubule (DCT) labelled. The cortical collecting duct (CCD) and inner medullary collecting duct (IMCD) are also shown. On the right, is a short-loop nephron with the short-loop descending thin limb (sDTL) labelled. The short loop nephron also has a PT, TAL and DCT, but they are not labelled (11).

These different nephron segments and blood vessels have unique properties that contribute to the different processes that occur in the different regions of the kidney. The kidney can be

divided into a superficial layer known as the cortex and an inner layer known as the medulla. Different processes take place in each layer, but in this study, attention will be given to the medulla, which plays an important role in urine concentration. The medullary region can be further divided into an outer and inner medulla. One nephron structure that is evident in both medullary regions is the loop of Henle. The loop of Henle is comprised of a descending thin limb (DTL), thick ascending limb (TAL) and ascending thin limb (ATL), each expressing different protein transporters and/or channels (Figure 2). In the outer medulla (OM), the DTLs and TALs engage in countercurrent multiplication. In addition, the TALs also play a role in active reabsorption. In the inner medulla, where DTLs and TALs are present, the steep osmotic gradient is hypothesized to be established through a combination of countercurrent multiplication like the outer medulla, but also relies more on passive processes rather than active (11). Other structures are present in medullary regions such as the renal capillaries, known as the ascending and descending vasa recta that play a role in countercurrent exchange to help maintain the osmotic gradients (10).

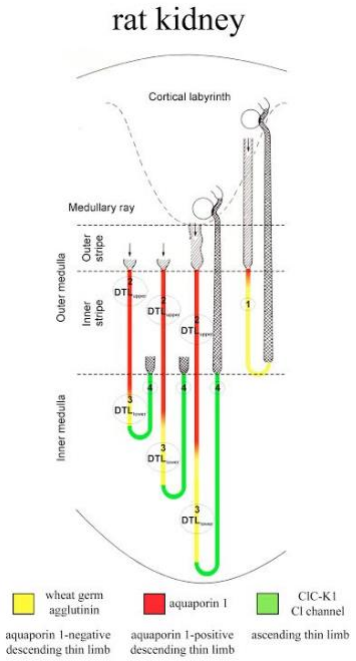

Figure 2. Diagram of the rat kidney showing the expression of several proteins including aquaporin-1 (AQP1) and chloride channel (ClC-K1) along the thin limbs of Henle's loops for long-loop and short-loop nephrons and their localization among the different regions of the medulla. Wheat germ agglutinin (WGA) is a lectin that nonspecifically labels all tubules and was used as a marker to delineate the AQP1-negative DTL (11).

One of the passive processes that takes place in the inner medulla involves transport of solutes via a paracellular pathway in different parts of the nephron, mediated by a family of tight junction proteins called claudins. Claudins are comprised of four transmembrane domains and charged amino acid residues that make them selective for specifically charged ions (15). The claudin that was examined in this study is claudin-4. Claudin-4 has been shown to localize to the ATLs and CDs in mouse kidneys (8). In the CDs, claudin-4 has been shown to interact with claudin-8 to increase permeability to chloride ions and may play a role in chloride reabsorption in collecting duct (CD) cells (6). A previous study used RNA interference to selectively knock down claudin-4 and claudin-8. As expected, the study showed that knocking down claudin-4, but not claudin-8 decreased chloride permeability in collecting duct cells (6). It also showed that knocking down claudin-8, but not claudin-4 resulted in a decrease in chloride conductance which indicates that claudin-8 interacts with claudin-4 to allow anions to move through the paracellular pathway in collecting duct cells (6). Because claudin-4 may be involved in chloride reabsorption, a defect in claudin-4 that renders it nonfunctional can potentially contribute to salt imbalances (4).

Another protein called SLC4A11 may also play a role in establishing concentration gradients in the medullary region through the process of solute recycling. These transporters are believed to be able to transport several substrates. Several studies suggest that SLC4A11 is

permeable to H+, NH3, and water (7,16). Mutations in SLC4A11 have been implicated in conditions such as congenital hereditary endothelial dystrophy (CHED) and Fuch's endothelial dystrophy (13). One study found that in the mouse kidney, SLC4A11 was localized to the DTLs using LacZ staining (5). Meanwhile, another study found that in the rat, SLC4A11 was localized to the inner medullary collecting ducts (IMCDs), DTLs in the outer medulla, and proximal tubules (PTs) (2). When the same antibody was used in human kidney tissue, SLC4A11 staining was found in the basolateral membrane of IMCDs, apical membranes of intercalated cells of the outer medullary collecting ducts (OMCDs) and IMCDs as well as the brush border of the PTs (2). Regarding this study, the expression of SLC4A11 was assessed in rat and mouse kidneys.

Although three-dimensional reconstructions of rodent kidneys have provided much insight into the architecture and function of the kidney, further information can be gleaned from generating three-dimensional reconstructions of porcine kidneys. Unlike the rat or mouse kidneys, the porcine kidney more closely resembles that of the human, and, similar to the human kidney, possesses a less prominent region known as the outer stripe of the outer medulla (OSOM) compared to that of both rodent kidneys (9,14). The architecture of the OSOM is not well characterized and some have suggested that this region is more susceptible to hypoxia, which can potentially contribute to acute kidney injury (1). This study will focus on using methods that have been previously used by Pannabecker et al. to generate three-dimensional reconstructions of the outer medulla of pig kidneys (12).

Methods

Slide and Tissue Preparation

Glass slides were prepared to accept tissue sections by cleaning using an acid alcohol solution consisting of 1% hydrochloric acid (HCl) in 70% ethanol. Slides were placed in a slide rack and immersed in 1:10 Poly-L-Lysine solution (Sigma Diagnostics) diluted with deionized water for 5 minutes. The slides were then drained and dried at room temperature overnight.

Kidneys were fixed in periodate-lysine-paraformaldehyde (PLP) in phosphate buffered saline (PBS) at 4℃, washed in PBS and immersed in an ethanol series. The ethanol series sequentially consists of two 30 minute immersions in 70% ethanol, one 30 minute immersion in 80% ethanol, one 30 immersion in 95% ethanol, three 30 minute immersions in 100% ethanol, three 30 minute immersions in xylene, a 90 minute immersion in 50:50 solution of xylene in melted paraffin wax at 58-60°C, a 90 minute immersion in 100% melted paraffin at 58-60°C, then followed by an overnight immersion in 100% melted paraffin wax in a vacuum incubator. After ethanol dehydration and paraffin infiltration, the tissues were embedded into paraffin blocks. Serial sections that were 4 µm thick were cut using an AO Spencer No. 820 rotary microtome and mounted on slides treated with Poly-L-Lysine.

Immunohistochemistry

Paraffin sections were deparaffinized through a series of three 3 minute xylene washes followed by a series of ethanol washes. The sequential order of the ethanol washes was two 2 minute washes in 100% ethanol, two 2 minute washes in 95% ethanol, two 2 minute washes in 70% ethanol and one 1 minute wash in distilled water. A PAP pen was then used to draw two parallel lines along two sides of the sections. The sections were then washed with 0.2% Triton X-100 (Sigma) in PBS for 2 minutes at room temperature and later washed with 1% SDS in PBS for 5 minutes. The sections were then washed with 0.2% Triton-X in PBS three times for 5 minutes

each time at room temperature. Afterwards, the slides were dried and 50 µL of blocking solution (BDT) consisting of 5% bovine serum albumin (BSA), 1% donkey serum, and 0.2% Triton-X in PBS was applied to each section for 10 minutes. The tissues were then placed in a slide box and stained overnight at 4°C using different combinations of primary antibodies diluted in 50 µL of the BDT solution (Fig. 3, 4, 5). These antibodies include antibodies raised against aquaporin 1 (AQP1), aquaporin 2 (AQP2), urea transporter B (UTB), plasmalemma vesicle associated protein (PV-1), chloride channel (CLC-K), claudin-4, and the solute carrier SLC4A11-2a. After the overnight application of the primary antibodies, the slides then underwent three 5 minute washes with 0.2% Triton-X in PBS. Different combinations of fluorescent-conjugated secondary antibodies were then diluted in BDT solution and 50 µL were applied to each slide for 2 hours at room temperature (Fig. 3, 4, 5). The secondary antibodies used included the fluorescent labels DAPI, FITC, TRITC, and Cy-5. Wheat germ agglutinin was also applied to some slides to label all the structures in the tissue. After the incubation in secondary antibodies, the sections underwent three 5 minute washes in 0.2% Triton-X in PBS. The sections were then mounted with Dako fluorescent mounting medium, coverslipped and imaged with epifluorescence microscopy (Applied Precision, DeltaVision). The images were then edited and analyzed using Photoshop and Amira.

Three-Dimensional Reconstruction of Serial Sections

The serial sections were aligned and then cropped using Photoshop to generate three stacks of serial images that capture immunofluorescence of AQP1, AQP2 and UTB in the serial tissue sections. AQP1 immunofluorescence delineates the AQP1-positive DTLs, AQP2 immunofluorescence delineates the CDs and UTB immunofluorescence delineates the DVRs.

Each stack of images was then manually position, using the Amira software, such that a given section was aligned with the section adjacent to it. The alignment process was repeated for each image in the stack. In the set of images within each stack, the tubules that display fluorescence were labeled with a graphical icon, a circle in this case, in a process called image segmentation. Amira then batch processed the icons to generate 3D reconstructions of the labelled tubules. Using image segmentation, three sets of digital reconstructions were generated, one for DTLs, CDs and DVRs. The digital reconstructions were then superimposed to produce a single 3D image of the region of interest (Fig. 14).

Primary Antibody	Host	Dilution	Source	Secondary Antibody	Dilution
Anti-AQP1	Mouse	1:100	Abcam	Donkey Anti-Mouse TRITC	1:200
Anti-AQP2	Goat	1:100	Santa Cruz	Donkey Anti-Goat DAPI (AMCA)	1:100
Anti-Claudin-4	Rabbit	1:25	InVitrogen	Donkey Anti-Rabbit Cy5	1:200
Wheat Germ Agglutinin/FITC	--	1:200	Vector	--	--
Anti-AQP1	Mouse	1:100	Abcam	Donkey Anti-Mouse FITC	1:200
Anti-AQP2	Goat	1:100	Santa Cruz	Donkey Anti-Goat DAPI (AMCA)	1:100
Anti-ClCK	Rabbit	1:100	Alomone	Donkey Anti-Rabbit Cy5	1:200
Anti-PV1	Chicken	1:200	Stan	Donkey Anti-Chicken TRITC	1:200

Anti-AQP1	Mouse	1:100	Abcam	Donkey Anti-Mouse FITC	1:200
Anti-AQP2	Goat	1:100	Santa Cruz	Donkey Anti-Goat DAPI (AMCA)	1:100
Anti-ClCK	Rabbit	1:100	Alomone	Donkey Anti-Rabbit Cy5	1:200
Wheat Germ Agglutinin/FITC	--	1:200	Vector	--	--
Anti-AQP2	Goat	1:100	Santa Cruz	Donkey Anti-Goat DAPI (AMCA)	1:100
Anti-PV1	Chicken	1:200	Stan	Donkey Anti-Chicken TRITC	1:200
Anti-UTB	Rabbit	1:25	--	Donkey Anti-Rabbit Cy5	1:200
Wheat Germ Agglutinin/FITC	--	1:200	Vector	--	--

Figure 3. Antibody panel showing combinations of antibodies used to label tissue sections on different slides for the experiments looking at the expression of Claudin-4 in the renal medulla.

Primary Antibody	Host	Dilution	Source	Secondary Antibody	Dilution
Anti-AQP1	Mouse	1:100	Abcam	Donkey Anti-Mouse TRITC	1:200
Anti-AQP2	Goat	1:100	Santa Cruz	Donkey Anti-Goat DAPI (AMCA)	1:100
Anti-SLC4A11-2a	Rabbit	1:100	Kurtz	Donkey Anti-Rabbit Alexa Fluor 488	1:100

Anti-AQP1	Mouse	1:100	Abcam	Donkey Anti-Mouse TRITC	1:200
Anti-AQP2	Goat	1:100	Santa Cruz	Donkey Anti-Goat DAPI (AMCA)	1:100
Anti-UTB	Rabbit	1:100	Sands	Donkey Anti-Rabbit Alexa Fluor 488	1:100
Anti-AQP1	Mouse	1:100	Abcam	Donkey Anti-Mouse TRITC	1:200
Anti-AQP2	Goat	1:100	Santa Cruz	Donkey Anti-Goat Cy5	1:100
Anti-SLC4A11-2a	Rabbit	1:100	Kurtz	Donkey Anti-Rabbit Alexa Fluor 488	1:100
Anti-AQP1	Mouse	1:100	Abcam	Donkey Anti-Mouse TRITC	1:200
Anti-AQP2	Goat	1:100	Santa Cruz	Donkey Anti-Goat Cy5	1:100
Anti-UTB	Rabbit	1:100	Sands	Donkey Anti-Rabbit Alexa Fluor 488	1:100
Anti-AQP1	Mouse	1:100	Abcam	Donkey Anti-Mouse FITC	1:200
Anti-AQP2	Goat	1:100	Santa Cruz	Donkey Anti-Goat DAPI (AMCA)	1:100
Anti-ClCK	Rabbit	1:100	Alomone	Donkey Anti-Rabbit Alexa Fluor 488	1:100

Figure 4. Antibody panel showing combinations of antibodies used to label tissue sections on different slides for the experiments looking at the expression of SLC4A11 in the renal medulla.

Primary Antibody	Host	Dilution	Source	Secondary Antibody	Dilution
Anti-AQP1	Mouse	1:100	Abcam	Donkey Anti-Mouse TRITC	1:200
Anti-AQP2	Goat	1:100	Santa Cruz	Donkey Anti-Goat Cy5	1:100
Anti-UTB	Rabbit	1:100	Sands	Donkey Anti-Rabbit Alexa Fluor 488	1:100
Anti-AQP1	Mouse	1:100	Abcam	Donkey Anti-Mouse TRITC	1:200
Anti-AQP2	Goat	1:100	Santa Cruz	Donkey Anti-Goat DAPI (AMCA)	1:100
Anti-ClCK	Rabbit	1:100	Alomone	Donkey Anti-Rabbit DAPI	1:100
Wheat Germ Agglutinin/FITC	--	1:200	Vector	--	--

Figure 5. Antibody panel showing combinations of antibodies used to label tissue sections on different slides for experiment involving the three-dimensional reconstruction of the pig outer medulla.

Results

Expression of Claudin-4 in Rat Inner Medulla

In the rat inner medulla, claudin-4 co-localizes with CDs which are labeled with AQP2 (Fig. 6). The expression of claudin-4 has a punctate appearance in that this protein is not uniformly labeled throughout the tubule. Closer inspection shows that claudin-4 is expressed in between the cells of the CDs, which is typical of tight junction proteins (Fig. 6). Claudin-4 is also expressed in tubules unlabeled with AQP1 or AQP2 (Fig. 6).

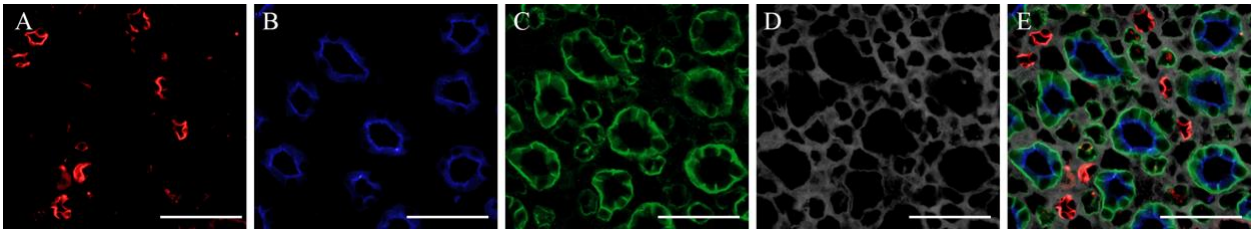

Figure 6. This panel of images come from a region of rat kidney tissue obtained from the inner medulla, near the papillary region. Panel A shows expression of AQP1 (red) which is associated with AQP1-positive DTLs. Panel B shows expression of AQP2 (blue) which is expressed in CDs. Panel C shows expression of claudin-4 (green). Panel D is wheat germ agglutinin (WGA) in gray. Panel E is a merge of panels A-D. All scale bars on the bottom right corner of each panel are 50 microns.

Further staining using an antibody against ClC-K1, a chloride channel expressed on ATLs, reveals that in addition to being expressed on CDs, claudin-4 is also expressed weakly on ATLs in a punctate manner (Fig. 7). Tubules that are not labeled with AQP1, AQP2 or ClC-K1 also seemed to express claudin-4 (Fig. 7).

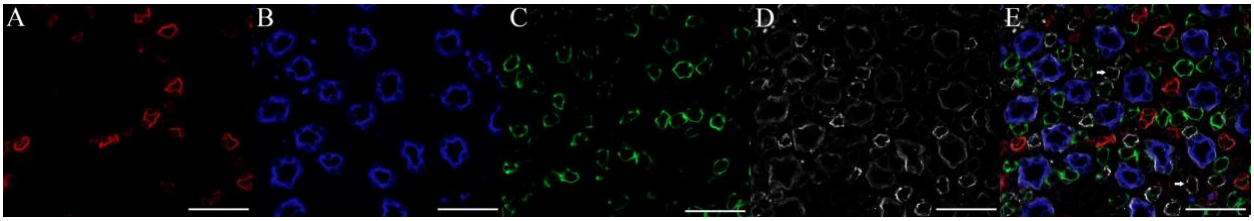

Figure 7. This panel of images comes from the rat inner medulla. Panel A shows expression of AQP1 (red). Panel B shows expression of AQP2 (blue). Panel C shows expression of ClC-K1 (green). Panel D show expression of claudin-4 (white). Panel E is a merge of panels A-D. Scale bars are 50 microns. White arrows point to tubules labeled by claudin-4 that do not co-localize with any of the antibodies used in this panel.

Additional staining showed that claudin-4 is not expressed in the kidney blood vessels. Antibodies against PV-1 and UTB were used to label for the ascending vasa recta (AVR) and descending vasa recta (DVR), respectively (Fig. 8). Claudin-4 did not co-localize with either antibody (Fig. 8). Thus, the tubules that claudin-4 strongly label that are not labeled with AQP1, AQP2, ClC-K1, PV-1, and UTB are likely AQP1-negative DTLs. There are no antibodies that have been found to selectively label these AQP1-negative DTLs in rat or mice.

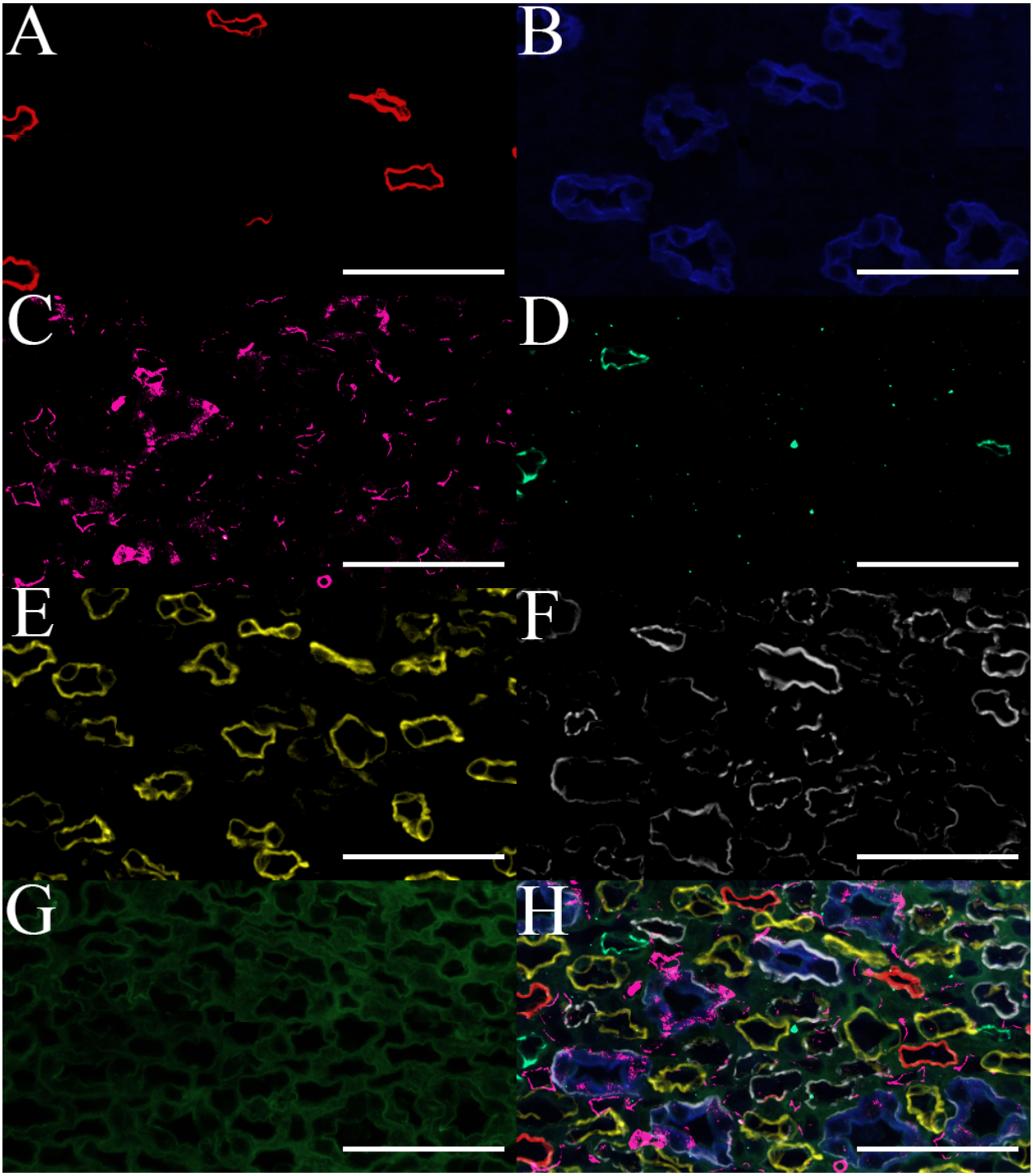

Figure 8. These panels of images were obtained from the rat inner medulla. Panel A shows expression of AQP1 (red). Panel B shows expression of AQP2 (blue). Panel C shows expression of PV-1 (pink). Panel D shows expression of UTB (ocean blue). Panel E shows expression of ClC-

K1 (yellow). Panel F shows expression of claudin-4 (white). Panel G shows expression of WGA (green). All scale bars are 50 microns.

Expression of SLC4A11 in Mouse and Rat Medulla

In the mouse ISOM, SLC4A11 co-localizes with AQP1, indicating that SLC4A11 is expressed in the long-loop AQP1-positive DTLs (Fig. 9). The expression of SLC4A11 in the AQP1-positive DTLs seem to be in the apical membrane (Fig. 10). SLC4A11 also appears to label the DVRs, labeled by AQP1 and UTB, but at a lower intensity compared to the AQP1-positive DTLs. Also, SLC4A11 seemed to label specific cells of the OMCDs not labeled with AQP2 which suggests that SLC4A11 may also be expressed on intercalated cells (Fig. 10).

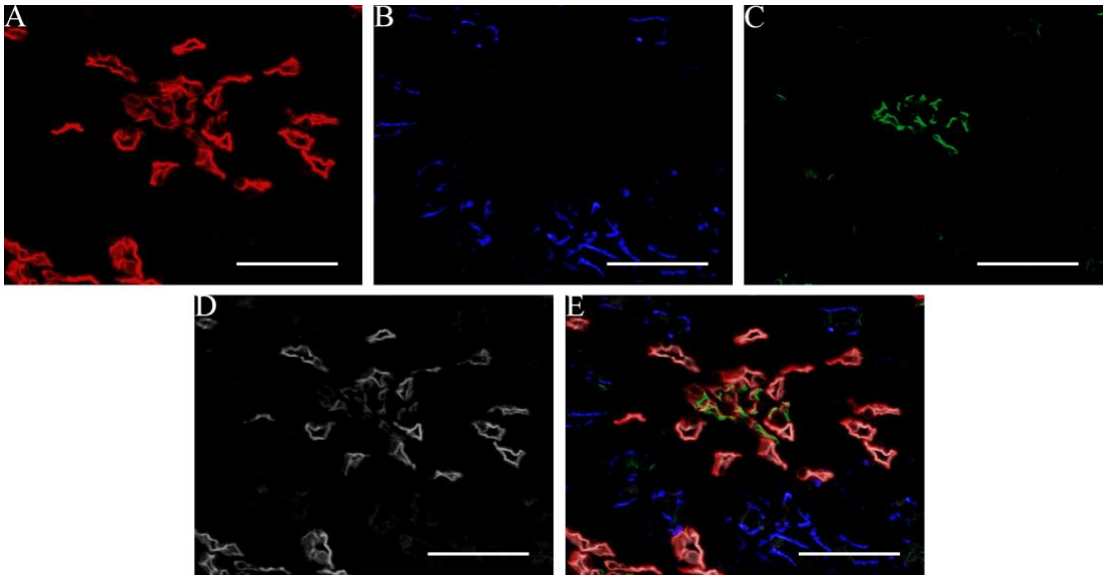

Figure 9. These are panels obtained from the same animal as Figure 9. Panel A is expression of AQP1 (red). Panel B is expression of AQP2 (blue). Panel C is expression of UTB (green). Panel D is expression of SLC4A11 (white). Panel E is a merge of panels A-D. The scale bars are 50 microns.

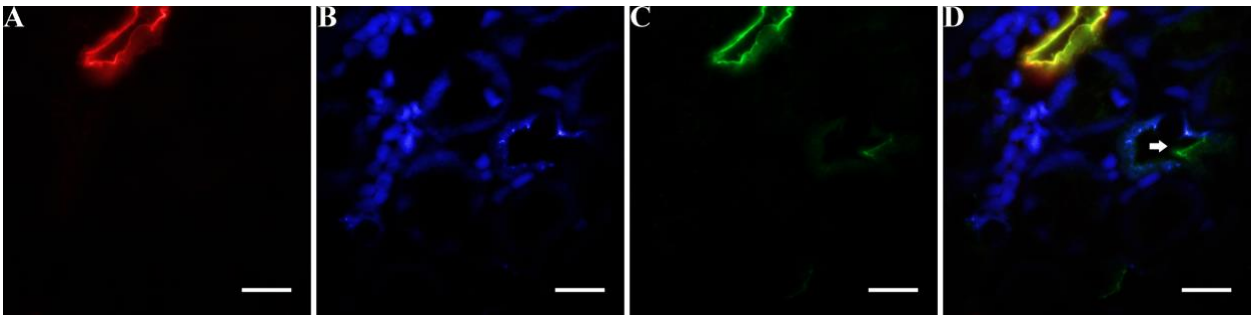

Figure 10. Expression of AQP1 (red) in panel A, AQP2 (blue) in panel B and SLC4A11 (green) in panel C in mouse OM at 100X magnification. Panel D is a merge of panels A-C. The white arrow is pointing to an intercalated cell in a CD. The scale bars are 10 microns.

In the mouse inner medulla (IM), SLC4A11 also appears to be expressed in the AQP1-positive DTLs, but there is little to no expression of SLC4A11 in the DVRs or the IMCDs (Fig. 11). Labelling with ClC-K1 also shows that SLC4A11 is not expressed in the ATLs (Fig. 11). Also, there is no detectable expression of SLC4A11 in the AQP1-negative DTLs since the SLC4A11 solely localized with the AQP1-positive DTLs.

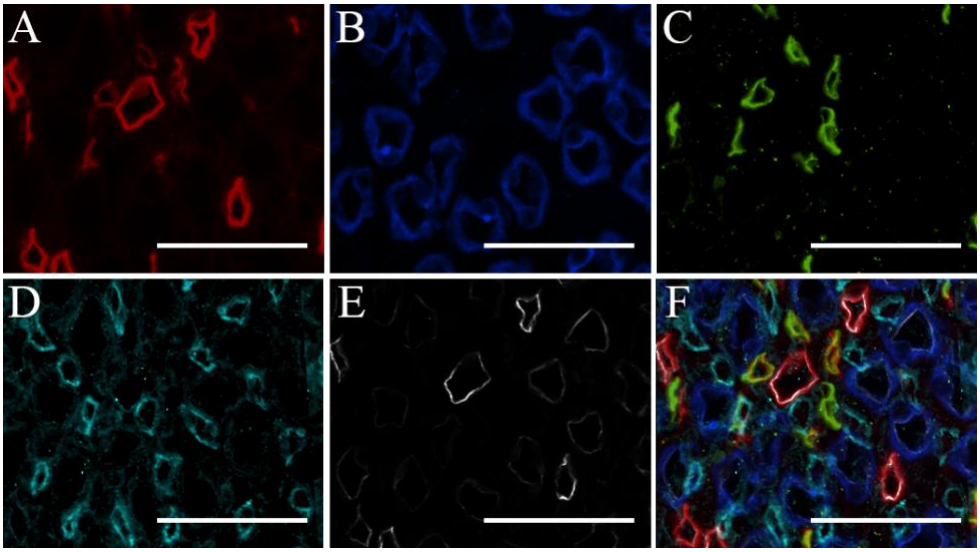

Figure 11. Expression of SLC4A11 in the mouse inner medulla. Panel A is expression of AQP1 (red). Panel B is expression of AQP2 (blue). Panel C is expression of UTB (green). Panel D is expression of ClC-K (ocean blue). Panel E is expression of SLC4A11 (white). Panel F is a merge of panels A-E. The scale bars are 50 microns.

The expression of SLC4A11 in the rat medulla appears solely in the AQP1-positive DTLs (Fig. 12). There appears to be little to no SLC4A11 expression in the IMCDs which express AQP2. Because SLC4A11 only co-localizes with AQP1-positive DTLs, it is not expressed in AQP1-negative DTLs, DVRs, or ATLs. The same pattern of expression is observed in the rat OM where SLC4A11 is expressed in tubules labeled with AQP1.

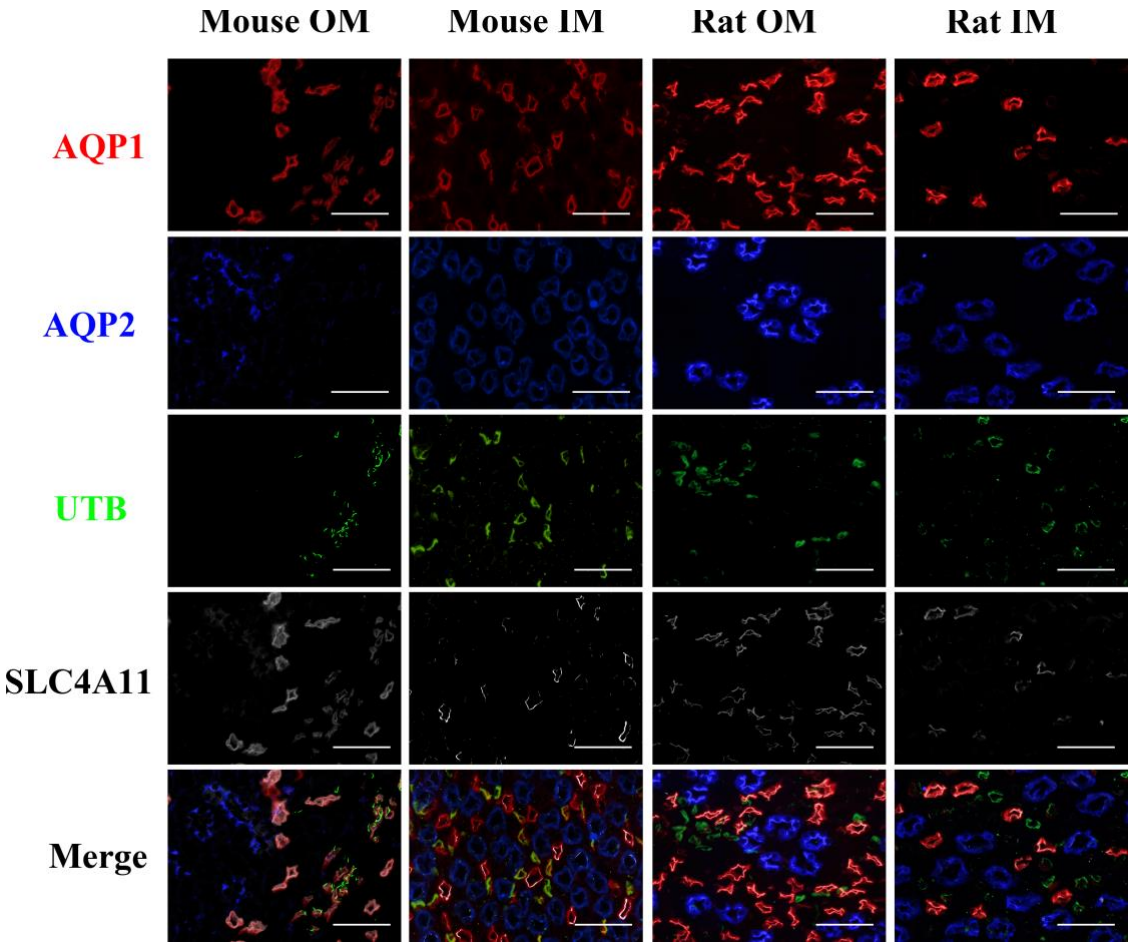

Figure 12. Comparison of SLC4A11 expression in IM and OM of mouse and rat. Red indicates AQP1 expression, blue AQP2, green is UTB and white is SLC4A11. The bottom panels are composites of the AQP1, AQP2, UTB and SLC4A11 panels. Scale bars are 50 microns.

Three-Dimensional Reconstruction of Pig Outer Medulla

Three-dimensional reconstruction of the pig OM was carried out in pig tissue that was obtained near the border of the cortex and medulla. The tissue sections were obtained from a region structurally comparable to the rat ISOM as indicated by the presence of AQP1-positive DTLs rather than thicker-walled proximal tubules (Fig. 13). CDs and DVRs are also present as indicated by the presence of structures that label with the AQP2 and UTB antibodies respectively (Fig. 13). The reconstruction focused on one of the vascular bundles present in the medulla which is why the DVRs are centrally located in the reconstruction (Fig. 13, 14). Because only a limited number of antibodies were used, not all the tubules were labelled, which is why there are gaps between the DVRs, AQP1-positive DTLs and OMCDs (Fig. 13). There are tubules that exist in these gaps such as AQP1-negative short-loop DTLs, AVRs and TALs (Fig. 15). A total of 77 serial sections were used to produce the 3D reconstruction.

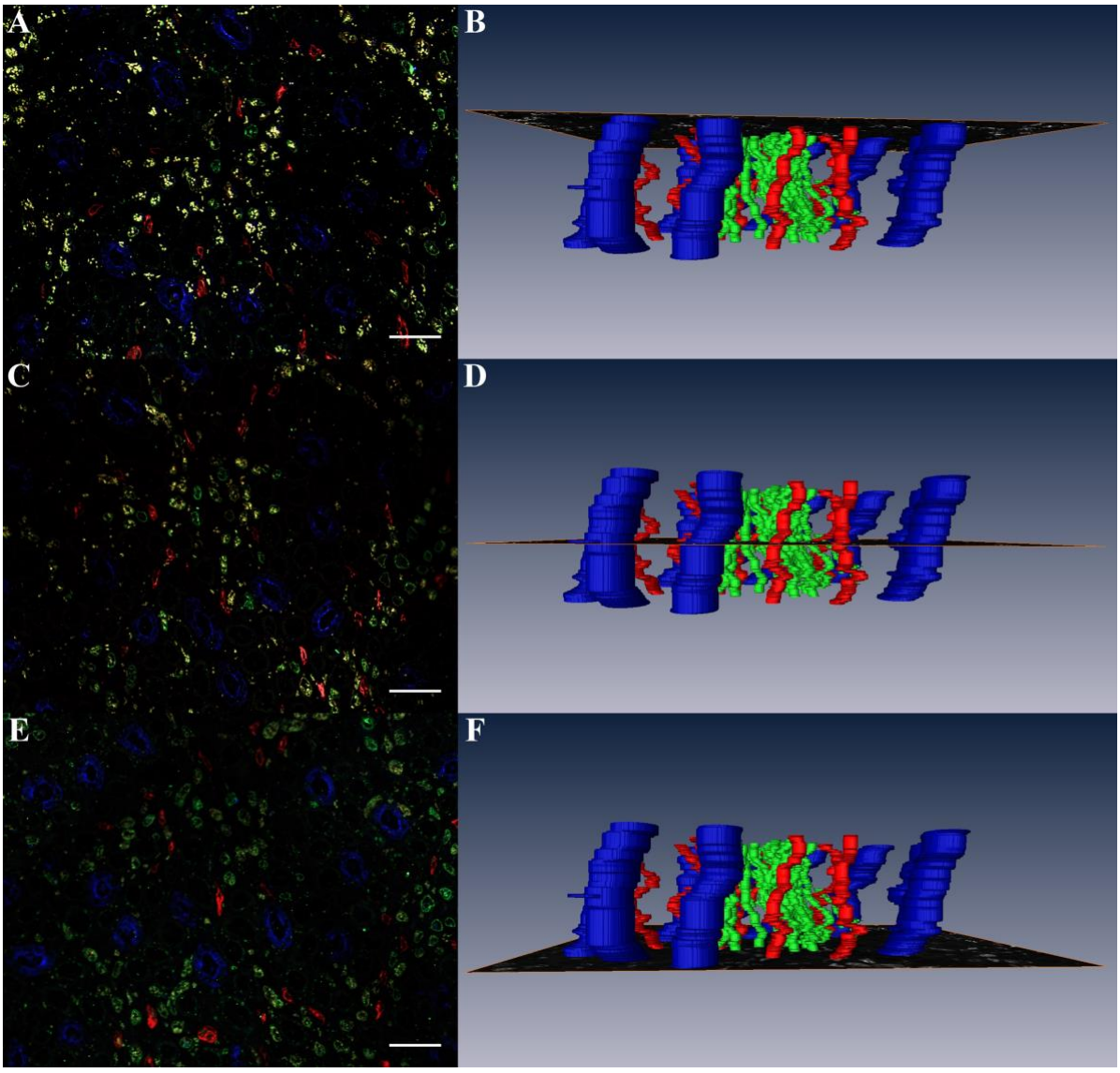

Figure 13. 77 serial sections were used to produce the 3D reconstruction of the pig kidney. Expression of AQP1 is in red, AQP2 is in blue and UTB is in green. Panel A shows a serial section that was used to generate the top layer as shown in panel B as the dark colored sheet. Panel A is the section that is most superficial. Panel C shows the serial section used to trace the middle layer shown in panel D. Panel E shows the serial section used to generate the bottom layer. The scale bars are 100 microns.

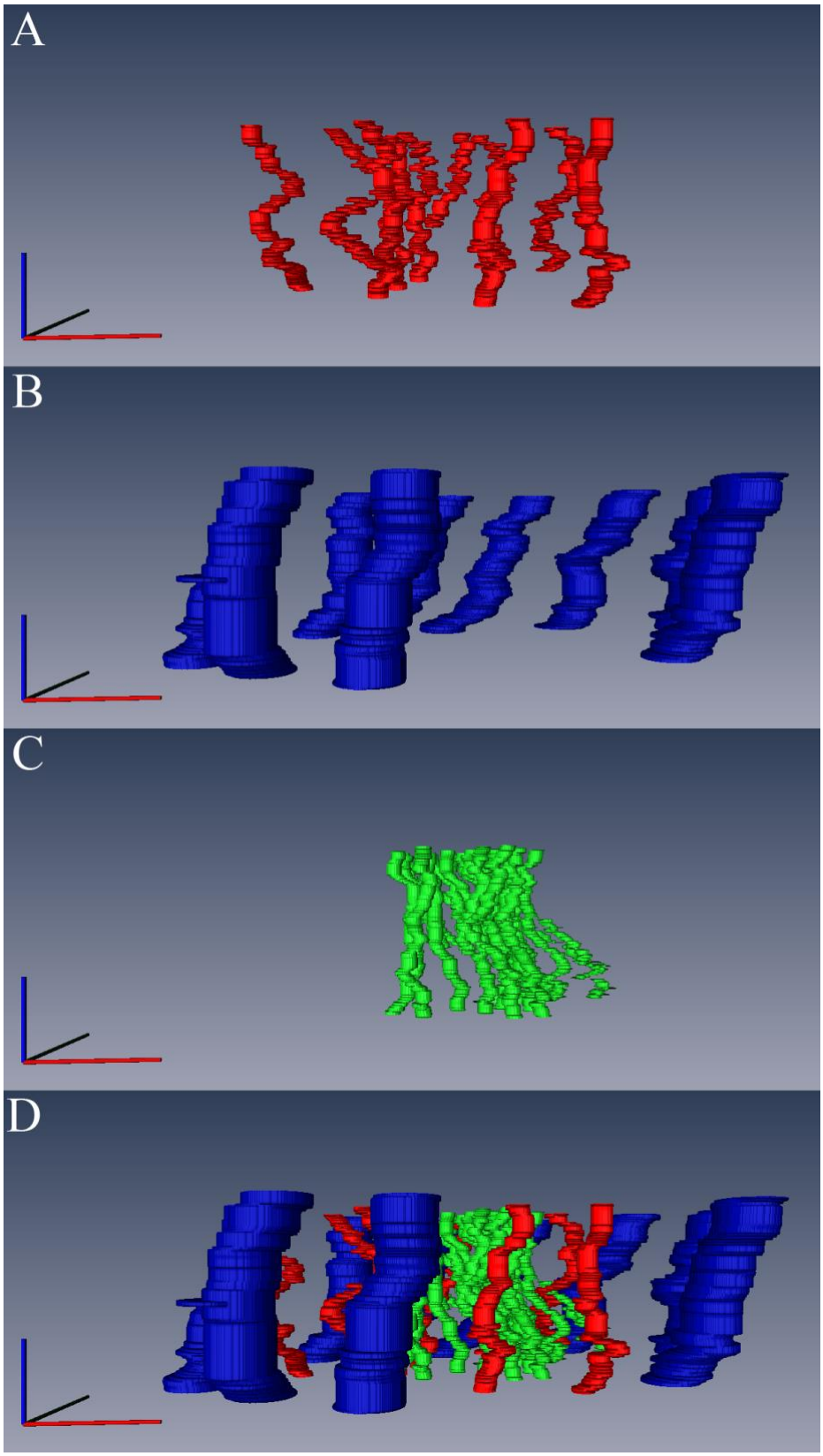
A
B
C
D

Figure 14: Multiple tubules were labelled for the 3D reconstruction. The reconstruction is organized so that the most superficial sections closer to the cortex are on top. Panel A shows the AQP1-positive DTLs (red) that were traced using the Amira software. Panel B shows the CDs (blue), which express AQP2. Panel C shows the DVRs (green), which express UTB. Panel D is a merge of panels A-C. The axis on the bottom left is 100 microns by 100 microns by 100 microns.

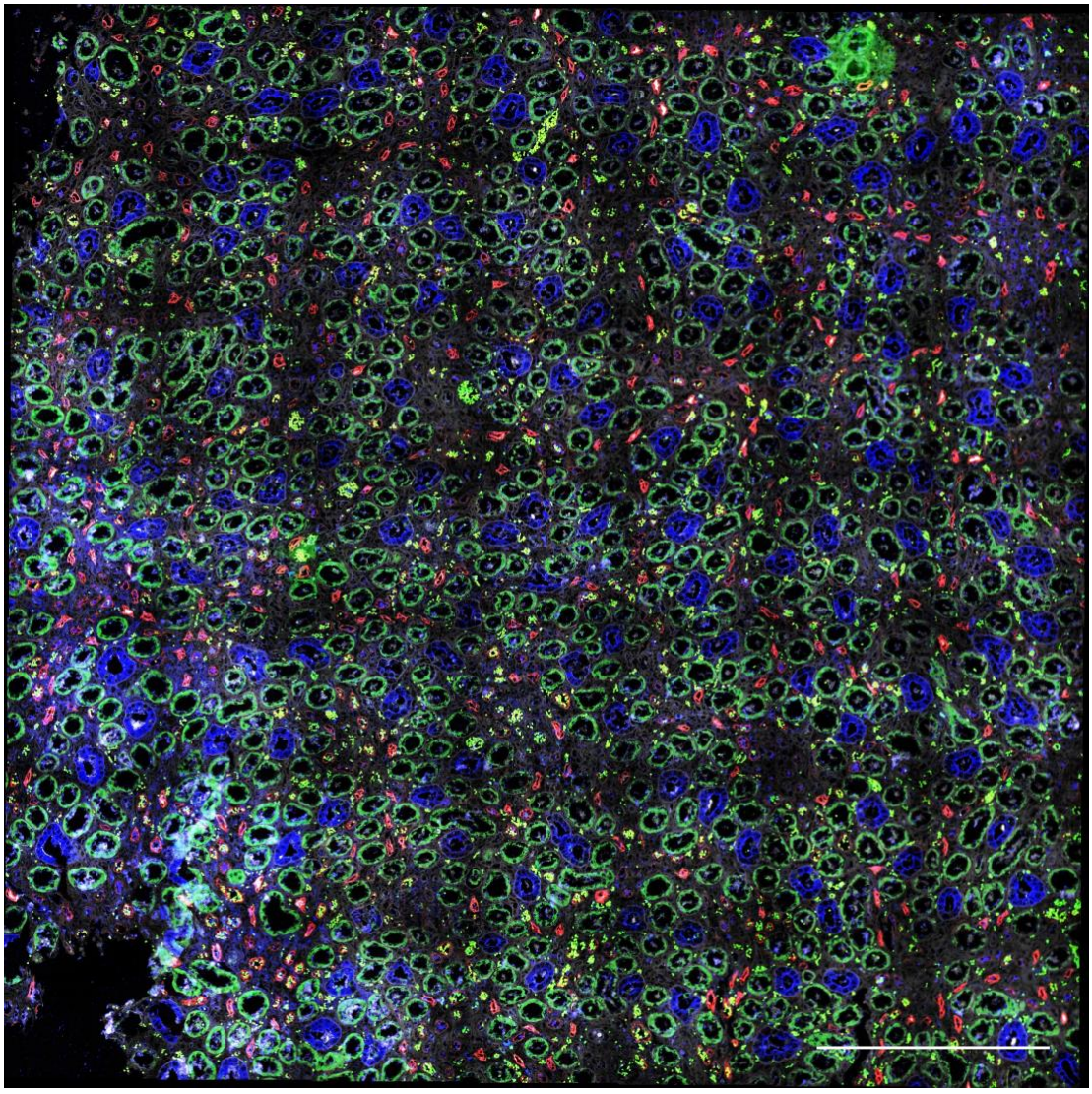

Figure 15. Pig renal medullary transverse tissue labeled with AQP1 (red), ClC-K (green), AQP2 (blue) and WGA (white). Scale bar is 1 millimeter.

Discussion

Claudin-4 in the Rat Renal Medulla

The findings from this study of claudin-4 support prior observations made about its expression in the rat IM, but also shows that claudin-4 may be expressed in other tubular structures of the IM. Claudin-4 is found to be expressed in the ATLs based on their co-localization with ClC-K and in the CDs based on their co-localization with AQP2. Other studies conducted in mice rather than rats have also found claudin-4 to be expressed in the ATLs and CDs (4, 8). In the study by Gong, it was noted that in the medulla of control mice, claudin-4 may be expressed in the AQP1-positive DTLs, but is absent in the TALs (4). In this study, there appeared to be little to no claudin-4 in the AQP1-positive DTLs. In addition to labelling CDs and ATLs, the claudin-4 antibody appeared to label other tubules in the inner medulla. Staining with PV1 and UTB antibodies labelling the AVRs and DVRs respectively showed no co-localization with claudin-4. Thus, in the rat IM, claudin-4 appears to also be expressed in AQP1-negative DTLs. It is uncertain whether this expression of claudin-4 in AQP1-negative DTLs is specific to rats.

On the basis of fluorescence intensity, claudin-4 appears to be most highly expressed in the AQP-1 negative DTLs as well as CDs relative to other tubular segments, which suggests that claudin-4 may be a relatively specific marker for the AQP1-negative DTLs. Based on previous studies (4, 8) and this study, claudin-4 not only serves as a tight junction but may potentially play an important role in the paracellular transport of solutes in the IM that helps to establish the osmotic gradients necessary for urine concentration. Na+ and urea transepithelial permeabilities in the AQP1-negative lower DTL are extremely high. We speculate that claudin-4 in the lower DTL is

potentially involved in transport of NaCl and/or urea, whose transport pathways in the DTL remain unknown (11).

SLC4A11 in the Mouse and Rat Renal Medulla

The results from the expression of SLC4A11 in the renal medulla support the view that the DTL is comprised of functionally distinct segments, the AQP1-positive DTLs that are found closer to the cortex and the AQP1-negative DTLs that are deeper in the medulla. As mentioned previously, several studies looked at the localization of SLC4A11 in mice, rats, and humans (2, 5). In one of the studies looking at mice, SLC4A11 was expressed in the DTLs, which was also observed in our data (5). Our results show that SLC4A11 co-localizes with AQP1 for both rats and mice. Thus, SLC4A11 is expressed in the AQP-1 positive segments of DTLs which are primarily present in the ISOM and upper part of the IM. In the rat and mouse IM, because SLC4A11 solely co-localizes with AQP1 and is not expressed in other tubular structures, SLC4A11 is not likely to be expressed in the AQP1-negative DTLs. In the OM of mice, SLC4A11 appears to be expressed in the DVRs and in the intercalated cells of OMCDs. In the rat OM, SLC4A11 is solely expressed in the AQP1-positive DTLs. In a different study looking at rats, the SLC4A11 was not only expressed in the DTLs, but was also observed to be present in the basolateral membrane of OMCDs, intercalated cells of OMCDs, and PTs (2). These differences in the data may reflect differences in methods of probing the tissue and interpreting the results.

Based on the expression of SLC4A11 observed in this study and findings from other studies that show SLC4A11 is permeable to ammonia, we hypothesize that in the OM, SLC4A11 expressed in the AQP1-positive DTLs may have a potential role in secretion and countercurrent multiplication of ammonia to help maintain the corticomedullary ammonia gradient (3,7,16).

SLC4A11 expression in the outer medullary DVR and absence in AVR suggests alternate pathways for ammonia recycling (3). The findings from this study provides further insight into the processes that contribute to an ammonia recycling mechanism in the renal medulla. The data for this SLC4A11 study has been published (3).

Reconstruction of the Pig Outer Medulla

The results from this experiment show that generating a 3D reconstruction of one of the vascular bundles in the pig ISOM is feasible. Antibody labeling of the tissue from this region revealed the presence of DTLs, CDs, DVRs and TALs. There appeared to be much space in between the DVRs, DTLs, and CDs of the vascular bundle examined. This space is most likely occupied by other tubules that have not been labeled as shown in a section taken from the same tissue that showed expression of ClC-K in segments that appear to be TALs based on their large diameters relative to the AQP1-positive DTLs.

Further studies can be performed that look at the diversity of nephron segments in the inner and outer regions of the porcine renal medulla. Additionally, further 3D reconstruction could be performed to better elucidate the architecture of the pig medulla. Importantly, the pathways for blood inflows and outflows (capillary architecture) in pig and human may be significantly different from rodents. This architecture could underlie different oxygenation dynamics in pig and human, and pig models may provide insights into why acute kidney injury in rodent models does not accurately recapitulate injury in the human and pig kidney (17). Such findings would provide key insights into functions of the outer medulla and how it is affected in a variety of renal diseases.

Acknowledgements

I thank the Undergraduate Biology Research Program (UBRP) at the University of Arizona for providing me the opportunity to work in a lab and providing financial assistance. I would like to thank Martha Nunez and Alejandro Lencinas from the lab of Dr. Raymond Runyan for teaching me how to embed and section tissue. I thank Dan Buster for answering any questions I have about the microscope used for these experiments and ensuring that the microscope is functioning. I would also like to thank Dr. Lukas, Dr. Whiteaker, Dr. George, Linda Lucero and the rest of lab staff at Barrow Neurological Institute for providing with a wonderful experience over two summers where I have learned more about the field of transport physiology. Finally, I would like to thank my thesis mentor, Dr. Pannabecker for his guidance and assistance throughout this project.

References

1. Brezis M, Rosen S. Hypoxia of the renal medulla–its implications for disease. *N Engl J Med* 332: 647-655, 1995.
2. Damkier HH, Nielsen S, Praetorius J. Molecular expression of SLC4-derived Na^+-dependent anion transporters in selected human tissues. *Am. J. Physiol Regul. Integr. Comp Physiol* 293: R2136–R2146, 2007.
3. Gee, MT, Kurtz, I, Pannabecker TL. Expression of SLC4A11 Protein in Mouse and Rat Medulla: A Candidate Transporter Involved in Outer Medullary Ammonia Recycling. *Physiol Rep* 8, in press. 2019.
4. Gong Y, Yu M, Yang J, et al. The Cap1-claudin-4 regulatory pathway is important for renal chloride reabsorption and blood pressure regulation. *Proc Natl Acad Sci U S A* 11: E3766–E3774, 2014.
5. Gröger N, Fröhlich H, Maier H, et al. SLC4A11 prevents osmotic imbalance leading to corneal endothelial dystrophy, deafness, and polyuria. *J Biol Chem* 285: 14467–14474, 2010.
6. Hou J, Renigunta A, Yang J, Waldegger S. Claudin-4 forms paracellular chloride channel in the kidney and requires claudin-8 for tight junction localization. *Proc Natl Acad Sci U S A* 107:18010–18015, 2010.
7. Kao L, Azimov R, Shao XM, et al. Multifunctional ion transport properties of human SLC4A11: comparison of the SLC4A11-B and SLC4A11-C variants. *Am J Physiol Cell Physiol* 311: C820–C830, 2016.

8. Kiuchi-Saishin Y, Gotoh S, Furuse M, Takasuga A, Tano Y, Tsukita S. Differential expression patterns of claudins, tight junction membrane proteins, in mouse nephron segments. *J Am Soc Nephrol* 13: 875–886, 2002.
9. Kriz W. Structural organization of the renal medulla: comparative and functional aspects. *Am J Physiol Regul Integr Comp Physiol* 241: R3–R16, 1981.
10. Pallone TL, Turner MR , Edwards A , Jamison RL . Countercurrent exchange in the renal medulla. *Am J Physiol Regul Integr Comp Physiol 284*: R1153–R1175, 2003.
11. Pannabecker TL. Comparative physiology and architecture associated with the mammalian urine concentrating mechanism: role of inner medullary water and urea transport pathways in the rodent medulla. *Am J Physiol Regul Integr Comp Physiol* 304: R488–R503, 2013.
12. Pannabecker TL, Dantzler WH. Three-dimensional architecture of collecting ducts, loops of Henle, and blood vessels in the renal papilla. *Am J Physiol Renal Physiol* 293: F696–F704, 2007.
13. Vithana E. N., Morgan P., Sundaresan P., et al. Mutations in sodium-borate cotransporter *SLC4A11* cause recessive congenital hereditary endothelial dystrophy (CHED2). *Nature Genetics* 38: 755–75, 2016.
14. Wei G, Rosen S, Dantzler WH, Pannabecker TL. Architecture of the human renal inner medulla and functional implications. *Am J Physiol Renal Physiol* 309: F627-F637, 2015.
15. Yu A. S. Claudins and the kidney. *Journal of the American Society of Nephrology: JASN 26*: 11–19, 2014.
16. Zhang W, Ogando DG, Bonanno JA, Obukhov AG. Human SLC4A11 is a novel NH_3/H^+ co-transporter. *J Biol Chem* 290: 16894–16905, 2015.

17. Zuk, A. & Bonventre, J. V. Acute kidney injury. *Annu. Rev. Med* 67: 293–307, 2016.